Identification of Frequency-Dependent Loudspeaker Cone Material Parameters using Inverse FEM

Alexander Ramirez

Dynaudio R&D
alera@dynaudio.com

Rubén Picó Vila

IGIC, Universitat Politècnica de València
Gandia, Spain
rpico@upv.edu.es

Francisco Castells Ramón

Instituto ITACA, Universitat Politècnica de València
Valencia, Spain
fcastells@eln.upv.es

Abstract**—** Accurate finite-element (FE) simulation of a loudspeaker requires the complex, frequency-dependent elastic properties of its soft moving parts, yet these are rarely available to the designer, who typically assumes a single value of Young's modulus, Poisson's ratio and isotropic loss factor for each component. This is usually adequate in the piston band but breaks down in the cone break-up region, because materials such as polypropylene (PP) and paper are viscoelastic and their stiffness and damping vary with frequency. This work estimates the frequency-dependent Young's modulus $E(f)$ and isotropic loss factor $\eta(f)$ of the PP cone of a 200 mm woofer by an inverse FE approach. A 2D axisymmetric vibroacoustic model is built in COMSOL Multiphysics 6.4, coupling Solid Mechanics to Pressure Acoustics through an acoustic–structure boundary; the air domain is truncated by a perfectly matched layer, an exterior-field calculation recovers the pressure at the measurement distance, and the magnetic motor is replaced by a calibrated lumped-element (R_2L_2) drive solved as a global algebraic equation coupled to the structure. Baseline linear and suspension parameters are obtained from Klippel LPM and electrical-impedance measurements, while the on-axis sound pressure level (SPL) from a 2π Klippel TRF measurement at approximately 31.5 cm is used as the optimization target. The identification proceeds in two numerical stages: the suspension parameters are found by matching the simulated complex eigenfrequency to the measured resonance frequency and quality factor, and the cone parameters are fitted band by band around five break-up modes by minimising the SPL residual, in both cases with the derivative-free BOBYQA optimizer. A sensitivity analysis confirms that the cone stiffness and damping dominate the high-frequency response. Although the SPL is an indirect observable of the cone vibration—measured only after acoustic propagation, so that the curve is affected by reflections, acoustic cancellations and baffle diffraction—it is far more accessible than laser-scanning vibrometry, which motivates its use as the optimization target. The optimization recovers frequency-dependent cone parameters that improve the agreement between the simulated and measured response relative to a constant-parameter model.

Index Terms**—** loudspeaker modelling, finite element method, inverse method, viscoelastic materials, material parameter identification, polypropylene cone, COMSOL.

I. Introduction

A. Problem description

The cone is the principal radiating element of a moving-coil loudspeaker and the dominant contributor to its acceleration—and therefore pressure—response, particularly at high frequencies above the so-called break-up region. Below break-up the cone moves essentially as a rigid piston; above it the cone flexes into a sequence of structural resonances (break-up modes) whose frequencies and amplitudes are governed by the cone's mass distribution, geometry and, critically, its elastic and damping properties. A finite-element model that assigns the cone a single, frequency-independent Young's modulus reproduces the piston band well but fails in the break-up region; in particular, the frequencies at which the break-up modes

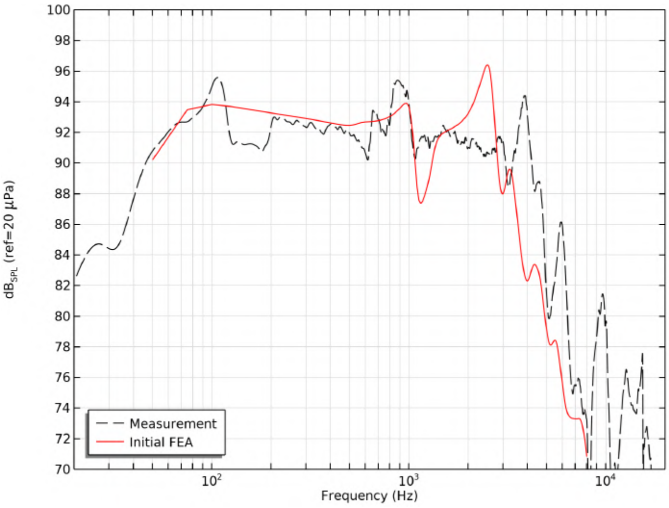

Figure 1: Motivation: a constant-modulus FE model matches the piston band but misplaces the cone break-up modes.

occur cannot be placed correctly with a constant modulus.

The reason is that real cone materials—polypropylene (PP), paper and similar polymers—are *viscoelastic* rather than purely elastic. Under dynamic loading their mechanical response combines an energy-storing (elastic) part and an energy-dissipating (viscous) part, and both depend on the rate of deformation, i.e. on frequency. This is described by a complex Young's modulus [1], [2],

$$E^*(\omega) = E'(\omega)\left[1 + \mathrm{i}\,\eta(\omega)\right], \qquad \eta = \frac{E''}{E'}, \tag{1}$$

where the storage modulus $E'(\omega)$ represents the effective stiffness and sets the resonance frequencies, while the loss factor $\eta(\omega)$ represents internal damping and controls how sharp and how high each resonance peak is. Writing $E(f)$ and $\eta(f)$ emphasises that both are functions of frequency. A helpful intuition is a viscoelastic polymer such as "silly putty": struck quickly it is stiff and elastic (it bounces), pulled slowly it flows—its apparent stiffness depends on how fast it is deformed. The cone material behaves analogously, so its effective stiffness and damping near 3 kHz are not the same as near 100 Hz; assuming them constant is precisely what misplaces the simulated break-up modes (Fig. 1). The subject of this study is a 200 mm (8-inch) woofer with a polypropylene cone.

B. Background and state of the art

Finite-element simulation becomes a useful tool in transducer design only if it reproduces the behaviour of the real loudspeaker with sufficient accuracy. While geometry and material densities are known early in the design, the elastic properties of the soft parts at higher frequencies are not: standard low-frequency coupon tests (e.g. ASTM E756 [3], performed on a small beam sample excited near its fundamental resonance) do not describe the assembled component, because soft materials such as paper, rubber, fabric and plastic are strongly frequency- and temperature-dependent, and because forming and gluing during assembly change their effective properties [4]. The defining input a good FE model lacks is therefore the complex, frequency-dependent Young's modulus—that is, both the storage modulus $E(f)$ and the loss factor $\eta(f)$ of (1)—of the cone and suspension as assembled.

Cardenas and Klippel addressed this by fitting an FE model to laser-vibrometry measurements of an existing prototype, recovering the complex modulus as a function of frequency [4]. Their work validated the simulation and identified the cone and soft parts as decisive for the higher-order modes after break-up; the related nonlinear intermodal-coupling work extends the same modelling philosophy [5]. The underlying distributed-parameter measurement and diagnostic framework—laser scanning of the radiator surface and decomposition of its vibration—was established by Klippel and Schlechter [6], [7]. The present work addresses essentially the same problem as Replogle [8], who quantified the influence of cone and surround materials on FE accuracy and optimized material properties against measurements; the FE-in-loudspeaker-design groundwork of Spatafora *et al.* [9] and the automated, surrogate-model calibration of Kim *et al.* [10] pursue closely related goals, as does the material- and shape-optimization study of Nielsen [11].

This thesis follows the Cardenas methodology but implements it in COMSOL and, crucially, replaces the laser-vibrometry target with the *on-axis SPL* measured by a Klippel TRF system in 2π conditions. Fitting the SPL is more difficult, because it conflates the mechanical response with acoustic effects (reflections, cancellations and baffle diffraction); the trade-off is accessibility, since the on-axis SPL can be obtained without a laser-scanning vibrometer. The structural-dynamics and modal background draws on classical treatments of plate vibration [12], cone vibration and sound radiation [13], modal testing [2], FE model updating [14], SVD-based modal analysis [15] and the accuracy of modal-parameter estimation [16], together with material surveys for transducer diaphragms [17] and laser-Doppler characterization of compliant materials [18].

C. Objectives

The goals of this work are: (i) to identify the frequency-dependent Young's modulus $E(f)$ and isotropic loss factor $\eta(f)$ of the PP cone by inverse FE fitting to the measured on-axis SPL; (ii) to establish reliable baseline and suspension parameters (spider, surround) from Klippel LPM and electrical-impedance measurements as a foundation for the cone identification; (iii) to validate the identified $E(f)$ and $\eta(f)$ in a full vibroacoustic forced-response simulation against measurement; and (iv) to assess whether the on-axis SPL—an accessible quantity, but one that observes the cone vibration only indirectly through the acoustic

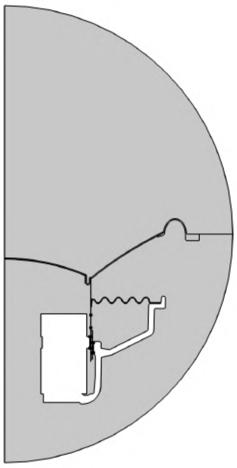

Figure 2: Two-dimensional axisymmetric model geometry of the 200 mm woofer.

environment—is a viable optimization target, so that the resulting curves can inform future cone designs.

II. Materials and Methods

A. Software and modules

The model was built in COMSOL Multiphysics 6.4 [19] using the Solid Mechanics and Pressure Acoustics (Frequency Domain) interfaces, the Global ODEs and DAEs interface, the General Optimization interface, and the Acoustic–Structure Boundary multiphysics coupling.

B. Model geometry

The geometry is a meridian (axisymmetric) section of the 200 mm woofer, shown in Fig. 2. Small glue regions are modelled at the surround–membrane, cone–former and former–spider interfaces. The cone is split into three parts so that it can be meshed with mapped (structured) domains. A half-sphere surrounds the driver to represent the air domain, and two small air domains inside the magnetic gap are reserved for a narrow-region-acoustics boundary condition. The pole pieces, magnet and basket are removed from the geometry, since the magnetic-fields physics is not included in this simulation. A line separating the top and bottom of the driver reproduces the 2π (half-space) radiation condition of the experimental measurement.

C. Materials

Table I lists the material assigned to each part together with its density, Young's modulus, isotropic loss factor and Poisson ratio. The cone values are the constant baseline that is later replaced by the identified $E(f)$ and $\eta(f)$.

Densities were estimated by weighing the real parts. In the geometry the coil is drawn as a single block of copper, whereas the real coil is a bundle of copper wires filled with resin; the copper density is therefore scaled by a factor so that the modelled coil matches the measured mass. The Young's modulus of the former and coil is taken directly from the COMSOL material database, as these parts have little influence on the result. The E and η of the surround were measured at low frequency with a DMA-type device, providing a good initial guess; these values, together with the E and η of the spider, were then refined in COMSOL against real measurements.

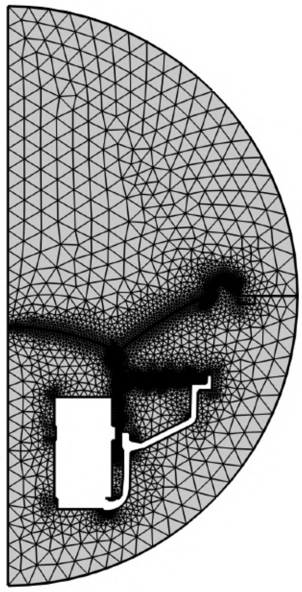

Figure 3: Finite-element mesh of the axisymmetric model: free triangular mesh in the air domain and over the structural parts, with finer elements near the driver components.

The suspension parameters were identified in two stages from electrical-impedance measurements. A real sample with its surround cut away was measured in Klippel to obtain its electrical impedance; in COMSOL the driver was modelled with the spider as the only suspension part and an optimization was run to find the E and η of the spider that reproduce the measured impedance. The surround was then added back and the optimization repeated, fine-tuning the surround E and η against the impedance of the complete driver.

D. Mesh

The cone was meshed with a mapped mesh to maximise element homogeneity; the coil and former, having simple shapes, were also mapped. The remaining domains, including the air, used a free triangular mesh (Fig. 3). Its element size was bounded by the acoustic wavelength $\lambda = c/f_{\max}$, with $c = 343\,\mathrm{m\,s^{-1}}$ and $f_{\max}$ the highest simulated frequency: the maximum element size was set to $\lambda/6$ and the minimum to $\lambda/20$. These limits were chosen primarily for the air domain and reused for the structural domains meshed with triangular elements.

Table I: Material properties assigned to the model parts. Cone values are the constant baseline (replaced by $E(f), \eta(f)$ in the validation study). Surround and spider E, η are identified from impedance; former and coil values are taken from the COMSOL library.

Part	Material	Density ($\mathrm{kg\,m^{-3}}$)	Young's modulus	Loss factor η	Poisson ν
Surround	Rubber	1170	27 MPa	0.162	0.47
Membrane (cone)	PP	945	3.4 GPa	0.164	0.33
Former	Aluminium	2705	69 GPa	0.001	0.33
Coil	Copper	8960	110 GPa	0.001	0.35
Spider	Cloth	555	0.57 GPa	0.32	0.33

E. Physics interfaces and boundary conditions

Solid Mechanics: All parts are modelled as linear elastic materials with isotropic loss-factor damping (the complex modulus of (1)). A fixed constraint is applied where the spider and surround are normally clamped. For the forced response, the magnetic motor is replaced by a lumped approximation of the driving force, which simplifies the model with negligible effect on the result:

$$F = Bl\, I_{\mathrm{coil}}, \tag{2}$$

where Bl is the force factor of the motor and I_{coil} the coil current. This force is applied as an axial body load distributed over the coil domain.

Electrical drive (lumped model): The electrical side of the transducer is introduced into the FE model as a lumped circuit equation solved simultaneously with the structural problem. The coil current is obtained from a lumped R_2L_2 model of the driver's electrical impedance (Fig. 4),

$$-V_0 + I_{\mathrm{coil}}\, Z_e + Bl\,(\mathrm{i}\omega)\,\overline{w}_{\mathrm{coil}} = 0, \tag{3}$$

$$Z_e = R_e + \mathrm{i}\omega L_e + \frac{\mathrm{i}\omega L_2 R_2}{R_2 + \mathrm{i}\omega L_2}. \tag{4}$$

Here V_0 is the prescribed input voltage; Bl, R_e, L_e, R_2, L_2 are taken from the Klippel LPM measurement; $\overline{w}_{\mathrm{coil}} =$ `coil_average(w)` is the average axial displacement over the coil domain (a non-local coupling) and `solid.iomega` $= \mathrm{i}\omega$, so that $Bl\,(\mathrm{i}\omega)\,\overline{w}_{\mathrm{coil}}$ is the motional back-EMF. Equation (3) is implemented as a single global algebraic equation in the Global ODEs and DAEs interface, with I_{coil} as its unknown; the resulting current is fed back into the body load of (2). Because the back-EMF depends on the structural displacement and the structural load depends on the current, the electromechanical drive is fully two-way coupled and is solved together with the Solid Mechanics problem in every frequency-domain study.

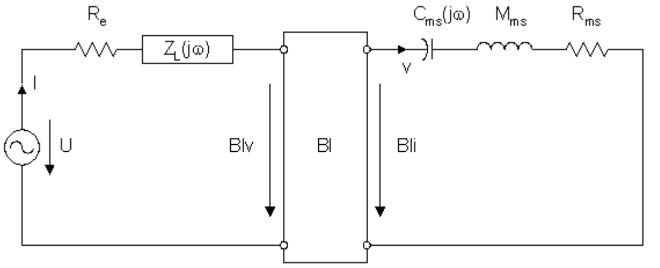

Figure 4: Lumped-element electrical model used to drive the structure (Eqs. (3)–(4)).

Pressure Acoustics: A perfectly matched layer (PML) is placed at the top and bottom boundaries of the half-sphere to absorb the outgoing acoustic waves. Because the half-sphere has a radius of 10 cm while the experimental data are measured at 31.5 cm, an exterior-field-calculation condition is applied on the same top boundary as the PML so that the pressure can be evaluated at the measurement distance. The spider is a woven cloth through which air passes, so a poroacoustics condition is applied to it; likewise, the real former has holes for heat and pressure relief that cannot be represented in a 2D axisymmetric geometry, so a section of the former is also assigned the poroacoustics condition.

F. Studies and solvers

Twelve studies were run in total; Table II summarises them, and the key ones are described below.

Study 1 — density calibration: A stationary Solid Mechanics study uses the model's mass properties to estimate the weight of each part, so the densities can be adjusted to match the real parts.

Studies 2a/2b — spider parameters: Study 2a estimates the baseline spider parameters E_0, η_0. The surround is omitted to match the experimental test, and only Solid Mechanics is used. Because the surrounding air adds a few grams to the perceived moving mass—visible in the measured impedance—an added-mass boundary condition is included, its value taken as the difference between the Klippel-measured mass (including air) and the simulated mass. The study combines an eigenfrequency analysis with a parameter optimization (BOBYQA), searching for a

Table II: Overview of the twelve COMSOL studies.

Study	Type	Purpose
1	Stationary (Solid)	Calibrate part densities against measured masses
2a	Eigenfrequency + optimization	Identify spider E_0, η_0 (no surround)
2b	Frequency domain	Verify spider result against measured impedance
3a	Eigenfrequency + optimization	Identify surround E, η (full suspension)
3b	Frequency domain	Verify full-suspension impedance
4	Frequency-domain sweep	Sensitivity analysis (six control variables)
5a	Frequency domain (vibroacoustic)	Full model, top + bottom air domains
5b	Frequency domain (vibroacoustic)	Top air domain only (justify reduction)
6	Eigenfrequency (Solid)	Identify the cone break-up modes
7–11	Frequency domain + optimization	Fit cone E, η at break-up modes 1–5
12	Frequency domain (validation)	Full model with $E(f), \eta(f)$

single eigenfrequency near the experimental one, with two objective functions

$$\mathrm{obj}_1 = \left|\,\mathrm{Re}(f_{\mathrm{eig}}) - f_s^{\mathrm{ns}}\right|^2, \tag{5}$$

$$\mathrm{obj}_2 = \left|Q_{\mathrm{eig}} - Q_{MS}^{\mathrm{ns}}\right|^2, \tag{6}$$

where $f_{\mathrm{eig}} =$ `comp2D.solid.freq` is the real part of the simulated complex eigenfrequency, $Q_{\mathrm{eig}} =$ `comp2D.solid.Q_eig` is the corresponding simulated modal quality factor, f_s is the measured fundamental (suspension) resonance frequency, Q_{MS} is the measured mechanical quality factor of that resonance (both from the Klippel LPM measurement), and the superscript "ns" denotes the no-surround experimental targets. Study 2b verifies the result: a forced frequency-domain step using the optimized values computes the electrical impedance for comparison with measurement.

Studies 3a/3b — surround parameters: Identical to Studies 2a/2b but with both surround and spider present, matching the E and η of the surround against the complete driver; the objective functions use the full-driver targets f_s and Q_{MS}.

Study 4 — sensitivity analysis: A frequency-domain sweep from 500 Hz to 8000 Hz in 25 Hz steps, with the area-weighted cone acceleration as objective,

$$\bar{a}_{\mathrm{cone}}(f) = \frac{\displaystyle\int_{\mathrm{cone}} 2\pi r \left|-(2\pi f)^2 w\right| \mathrm{d}r}{\displaystyle\int_{\mathrm{cone}} 2\pi r \,\mathrm{d}r}, \tag{7}$$

where the integrals are the non-local coupling `intop_cone` over the top boundary of the cone; the cone acceleration is proportional to the pressure response. The six control variables are the Young's modulus and isotropic loss factor of the cone, surround and spider. The analysis shows that the cone's Young's modulus has the strongest influence on the acceleration response, especially at the radial break-up modes, with the cone loss factor second; the spider has only minor influence, confirming the role of the cone identified by Cardenas [4].

Studies 5a/5b — air-domain reduction: Study 5a is the first complete vibroacoustic frequency-domain run using both the top and bottom air domains. Study 5b repeats it with only the top air domain; the computed pressures are very similar, so the bottom air domain is dropped from all subsequent studies to save computation (Fig. 7).

Study 6 — break-up mode identification: An eigenfrequency study (Solid Mechanics only) reveals the break-up modes of the complete system. Following Cardenas [4], material parameters can only be identified on the active parts, so it is necessary to know where the cone is in a resonant mode; an optimization is then run in the frequency band around each mode, where varying the cone parameters strongly affects the response. It is assumed that E and η depend on frequency but are constant within a small frequency band; the identified mode shapes are shown in Figs. 8 and 9.

Studies 7–11 — cone parameters per mode: Each of these is a frequency-domain study with a parameter-optimization step (BOBYQA), applied to one of the first five cone break-up modes. The objective in every case is the SPL residual

$$J(f) = \big(\mathrm{SPL}_{\mathrm{meas}}(f) - \mathrm{SPL}_{\mathrm{sim}}(f)\big)^2, \tag{8}$$

where $\mathrm{SPL}_{\mathrm{sim}} =$ `comp2D.SPL_probe`, evaluated over a manually selected band around the mode. The control parameters are the cone E and η, with manually set initial value and lower and upper bounds. The process is iterative and requires several passes to find the combination that best matches the measurement.

Study 12 — validation: Once the cone E and η have been found at each mode, they are assembled into continuous $E(f)$ and $\eta(f)$ curves using interpolation functions. These are assigned to the cone material and a full vibroacoustic forced-response analysis is run. The result shows an improvement over the model with constant E and η.

III. Theory

This section develops the physics underlying the simulation interfaces and the inverse identification. It covers the viscoelastic material model, the structural and acoustic field equations with their coupling and boundary conditions, the lumped electromechanical drive, the cone-vibration and radiation background, and the formulation of the two parameter-identification strategies together with a comparison of them.

A. Viscoelastic material model and structural damping

Cone polymers such as polypropylene (PP) are viscoelastic: under harmonic loading their response combines an elastic and a viscous part, captured by the complex Young's modulus of (1), $E^* = E'(1 + \mathrm{i}\eta)$, with storage modulus E' (effective stiffness) and loss modulus $E'' = \eta E'$ (dissipation). Across the audio band PP operates on the low-frequency flank of its principal relaxation, so E' and η vary slowly and monotonically with frequency; over the narrow band surrounding a single resonance they may therefore be treated as constant, which is the assumption that makes the per-mode identification well-posed. The isotropic loss factor is a hysteretic (structural) damping model: the element stiffness is scaled by $(1 + \mathrm{i}\eta)$, so the energy dissipated per cycle is independent of frequency within the band. This represents the weak frequency dependence of polymer damping better than viscous (Rayleigh) damping, which would force the loss to grow linearly with frequency.

B. Structural dynamics

In the frequency domain the linear-elastic equation of motion for the moving assembly is

$$\nabla\cdot\boldsymbol{\sigma} + \boldsymbol{F}_v = -\rho\,\omega^2\boldsymbol{u}, \qquad \boldsymbol{\sigma} = \mathsf{C}(\omega) : \boldsymbol{\varepsilon}, \tag{9}$$

where $\boldsymbol{u}$ is the displacement, ρ the density, $\boldsymbol{F}_v$ a body load and $\mathsf{C}(\omega) = (1 + \mathrm{i}\eta)\,\mathsf{C}_0$ the complex elasticity tensor built from $E'(\omega)$ and ν. The unforced, undriven problem is the complex eigenvalue problem

$$\big[(1 + \mathrm{i}\eta)\,\mathbf{K} - \omega^2\mathbf{M}\big]\,\boldsymbol{\phi} = \mathbf{0}, \tag{10}$$

whose complex eigenvalues yield, for each mode n, a natural frequency f'_n and a modal quality factor Q_n through $f_n = f'_n\big(1 + \mathrm{i}/2Q_n\big)$. For light damping $Q_n \approx 1/\eta$, so matching the simulated eigenfrequency and quality factor to the measured f_s and Q_{MS} (Studies 2a/3a, Eqs. (5)–(6)) constrains the storage modulus through f' and the loss factor through Q.

C. Acoustic field, coupling and boundary conditions

The air is governed by the Helmholtz equation for the acoustic pressure p,

$$\nabla\cdot\Big(-\tfrac{1}{\rho_0}(\nabla p - \boldsymbol{q}_d)\Big) - \frac{\omega^2}{\rho_0 c^2}\,p = Q_m, \tag{11}$$

with air density ρ_0, sound speed c, wavenumber $k = \omega/c$, and optional dipole/monopole sources $\boldsymbol{q}_d, Q_m$. On the wetted boundaries the structure and fluid are coupled by continuity of normal acceleration and by the pressure acting as a load on the solid,

$$-\boldsymbol{n}\cdot\Big(-\tfrac{1}{\rho_0}(\nabla p - \boldsymbol{q}_d)\Big) = \boldsymbol{n}\cdot\boldsymbol{a}, \qquad \boldsymbol{F}_A = p\,\boldsymbol{n}, \tag{12}$$

where $\boldsymbol{a} = -\omega^2\boldsymbol{u}$ is the structural acceleration. Four boundary conditions complete the acoustic model. A *perfectly matched layer* (PML) at the truncation of the half-sphere absorbs outgoing waves without reflection, emulating an unbounded domain. An *exterior-field calculation* applies the Helmholtz–Kirchhoff integral to p and its normal derivative on the outer boundary, so the pressure at the 31.5 cm measurement distance is recovered from the 10 cm mesh sphere. *Narrow-region acoustics* accounts for the viscous and thermal boundary-layer losses that dominate in the thin magnetic-gap air. Finally, the woven spider and the holed former section are represented as an equivalent fluid through a *poroacoustics* (Delany–Bazley) model, whose complex characteristic impedance and wavenumber,

$$Z_c = \rho_0 c\,\big[\,1 + a_1 X^{-a_2} - \mathrm{i}\,a_3 X^{-a_4}\,\big], \tag{13}$$

$$k_c = \frac{\omega}{c}\,\big[\,1 + b_1 X^{-b_2} - \mathrm{i}\,b_3 X^{-b_4}\,\big], \qquad X = \frac{\rho_0 f}{\sigma_f}, \tag{14}$$

depend on the flow resistivity σ_f and the empirical coefficients a_i, b_i, and introduce the frequency-dependent damping of air passing through the porous parts.

D. Electromechanical drive

The motor is reduced to the Lorentz force of (2), $F = Bl\,I_{\mathrm{coil}}$, with the coil current obtained from the lumped electrical model of (3)–(4). The parallel branch $R_2 \parallel \mathrm{i}\omega L_2$ represents the semi-inductance, i.e. the frequency-dependent voice-coil impedance produced by eddy currents in the conductive pole structure, while the term $Bl\,(\mathrm{i}\omega)\,\overline{w}_{\mathrm{coil}}$ is the motional back-EMF that couples the mechanical velocity to the electrical equation and closes the electromechanical loop. Since the magnetic field is essentially static and the gap geometry fixed, replacing the magnetic-fields physics by this calibrated lumped drive (parameters from the Klippel LPM measurement) has a negligible effect on the response while greatly reducing the model size.

E. Cone vibration and radiation

A cone is a curved shell that, below its first break-up, translates as a rigid piston and, above it, deforms into flexural modes. For a thin plate the flexural rigidity is

$$D = \frac{Eh^3}{12\,(1 - \nu^2)}, \tag{15}$$

and the modal frequencies scale as $f_n \propto \sqrt{D/\rho h} \propto \sqrt{E'}$; the storage modulus therefore sets the break-up frequencies, and an error in E' shifts them—the physical basis for identifying $E'(f)$ from the measured modal frequencies [12]. For sound radiation, the far-field on-axis pressure of an axisymmetric radiator is proportional to the surface integral of the normal acceleration (Rayleigh integral); when no acoustic cancellation occurs, the area-weighted acceleration tracks the SPL [13]. This justifies both the use of the area-weighted cone acceleration of (7) as the

Table III: Comparison of the two identification strategies.

	A: Eigenfrequency	**B: Forced-response SPL**
Observable	Complex eigenfrequency (f', Q)	On-axis SPL over a band
Studies	2a, 3a	7–11
Constrains	Suspension E, η via f_s, Q_{MS}	Cone E, η per mode
Optimiser	BOBYQA	BOBYQA
Strengths	Fast, robust, well-posed for an isolated mode	Uses the accessible acoustic output; captures frequency and amplitude
Limitations	Needs a clean dominant mode; matches resonance only	SPL artifacts; narrow-band, manual bounds; sparse sampling

sensitivity objective and the use of the on-axis SPL to identify the cone parameters.

F. Inverse problem and parameter identification

The identification seeks the material parameters $\boldsymbol{\theta} = \{E, \eta\}$ of each active part that minimise a least-squares residual between simulation and measurement. Identifiability follows the active-mode principle: a parameter is observable only where its part participates in the response [4]. The sensitivity analysis (Study 4) confirms that the cone dominates above break-up, so cone parameters are identified at the cone-dominated break-up modes, whereas the suspension parameters are identified at the low-frequency suspension-controlled resonance. Two complementary strategies are used. *Strategy A — eigenfrequency matching* (suspension; Studies 2a/3a) minimises the squared error between the simulated complex eigenfrequency and the measured f_s and Q_{MS} (Eqs. (5)–(6)). *Strategy B — forced-response SPL fitting* (cone; Studies 7–11) minimises the SPL residual of (8) over a narrow band around each break-up mode, yielding one (E, η) pair per mode that are interpolated into the curves $E(f)$ and $\eta(f)$ under the constant-within-a-band assumption. Both use the derivative-free BOBYQA optimiser, which suits the small number of variables per fit and objectives evaluated through COMSOL probe and integration operators that lack reliable analytic gradients.

The optimisation target is the measured on-axis SPL—a single far-field microphone response—rather than the full-surface laser-vibrometry velocity data used by Cardenas and Klippel [4], [6]. The SPL is the directly relevant and widely accessible observable; the trade-off is that it conflates the mechanical response with acoustic effects (reflections, cancellations, baffle diffraction). Table III compares the two strategies.

IV. Results and Discussion

A. Suspension parameter identification

Figure 5 shows the simulated and measured electrical impedance for the two configurations used to estimate the stiffness and damping of the suspension parts: the driver with the surround removed, Fig. 5(a), and the complete suspension, Fig. 5(b). Around the fundamental resonance the no-surround case agrees closely with the measurement, whereas the full-suspension case deviates more noticeably in the *amplitude* of the resonance peak, by approximately 6 dB. As both simulations were run with Solid Mechanics

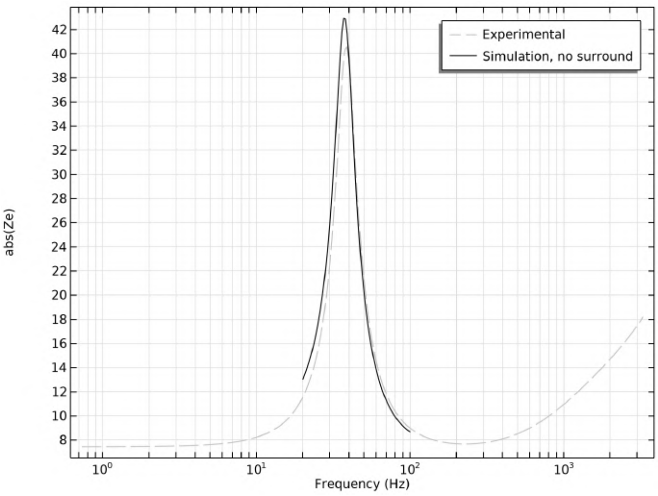

(a) Spider only (surround removed).

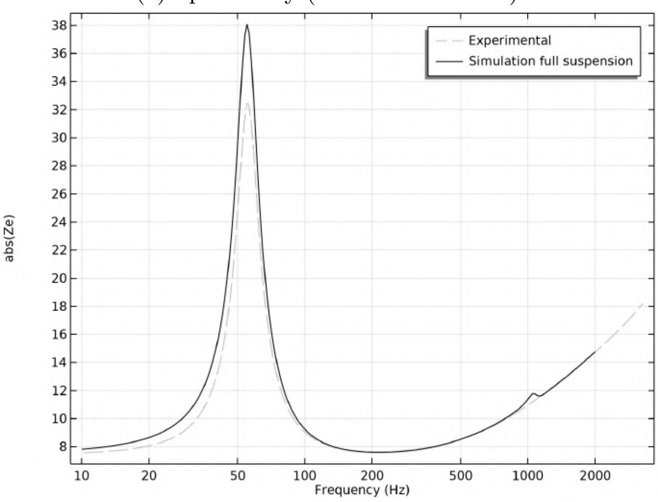

(b) Full suspension (spider + surround).

Figure 5: Measured versus simulated electrical impedance used to identify the suspension parameters (Studies 2b/3b).

only, this discrepancy is most plausibly attributed to the missing radiation resistance of the air, which would add damping and reduce the peak height. The lumped R_2L_2 model, by contrast, reproduces the measured impedance very well, as expected: the impedance is governed mainly by the lumped coil-current model (I_{coil}) rather than by the structural model.

B. Sensitivity analysis

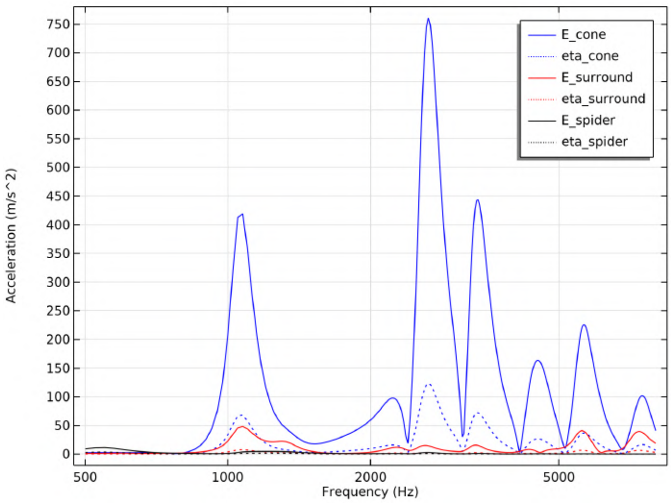

Figure 6: Sensitivity of the area-weighted cone acceleration to the six control variables across 500 Hz to 8000 Hz (Study 4); the cone Young's modulus is dominant.

Figure 6 confirms the hypothesis that the cone stiffness and damping are the most influential parameters on the response over the frequency range of interest. The surround and spider have a much smaller effect, but they are not entirely inactive; consequently, optimising for the cone E and η alone causes these two cone parameters to *absorb* the residual contributions of the suspension. The identified cone values are therefore effective parameters rather than intrinsic material constants.

C. Air-domain reduction

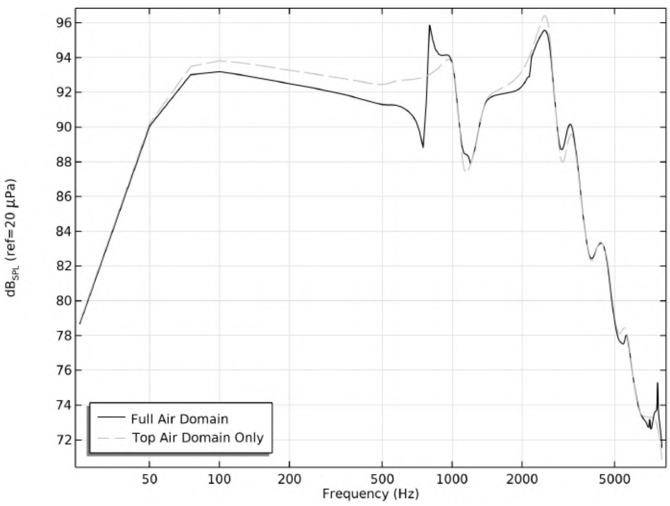

Figure 7: Computed on-axis pressure with both air domains versus the top air domain only (Studies 5a/5b); the close agreement justifies dropping the bottom domain.

Figure 7 compares a simulation using the full air domain with one using only the top air domain. The air on the rear side of the driver has little influence on the on-axis response, which supports neglecting the bottom air domain in the subsequent calculations to save computation time.

D. Break-up mode identification

Figures 8 and 9 show the radial break-up modes identified in the eigenfrequency study. Although the 2D axisymmetric geometry ignores all circumferential modes, the modal set still had to be inspected manually, since additional spider- and surround-dominated modes appear that are not of interest for the cone identification. Radial break-up modes contribute more strongly to the on-axis response of a loudspeaker than circumferential or other mode types [7], [13], which makes them the appropriate targets for the parameter fitting.

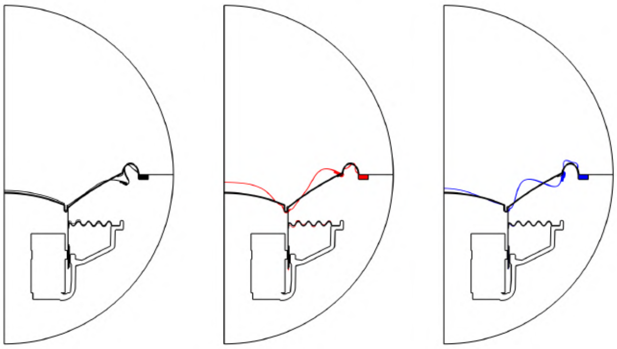

Figure 8: Radial cone break-up mode shapes, modes 1–3 (Study 6).

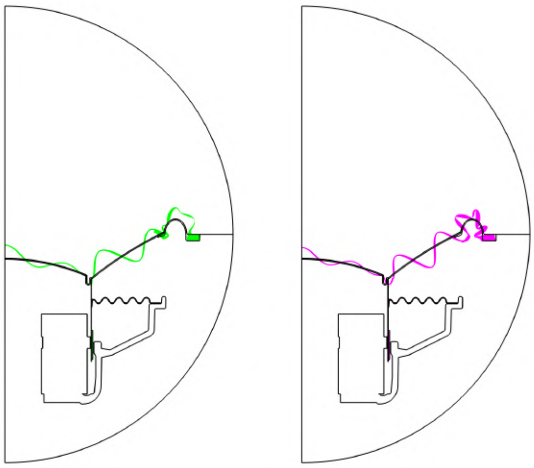

Figure 9: Radial cone break-up mode shapes, modes 4–5 (Study 6).

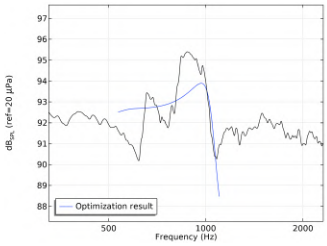

(a) Mode 1.

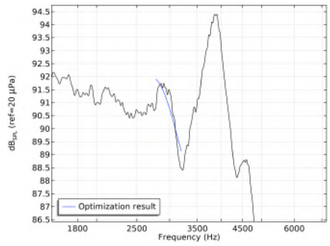

(b) Mode 2.

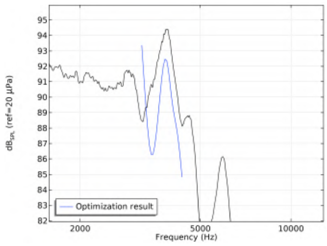

(c) Mode 3.

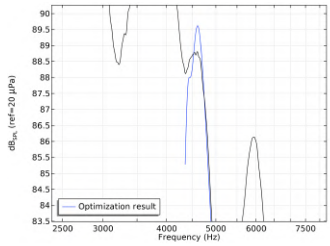

(d) Mode 4.

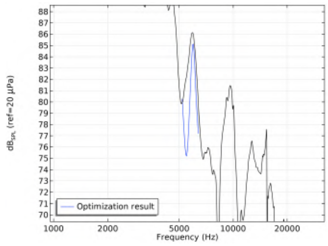

(e) Mode 5.

Figure 10: Measured versus simulated on-axis SPL around each of the five cone break-up modes after optimisation of the cone E and η (Studies 7–11).

E. Cone parameter identification

Figure 10 shows the converged optimisation result of Studies 7–11—the best fit obtained after the iterative BOBYQA passes—at each of the five break-up regions. The underlying assumption is that the Young's modulus and isotropic loss factor are constant over the narrow frequency band in which each break-up mode forms. The fits are not perfect, but each is an improvement over the use of a single constant value of stiffness and damping. Previous authors have argued that a more accurate identification can be obtained from cone-acceleration signals measured with a laser scanning vibrometer [4], [6]. Such an instrument is, however, expensive and specialised, whereas the on-axis SPL measured with a microphone is an accessible quantity that virtually every loudspeaker designer can obtain. The trade-off is that the SPL is a heavily processed quantity and is more susceptible to artefacts—sound reflections, diffraction at the baffle and microphone, and pressure cancellations, among others. It was therefore anticipated that the fit would be more difficult, particularly at higher frequencies, which is consistent with the larger residual mismatch observed for the upper modes.

F. Validation

Figure 11 shows the validation of the complete vibroacoustic model with the identified frequency-dependent parameters assigned to the cone (Study 12). Once the stiffness and damping values had been found by fitting the SPL at the radial break-up modes and assembled into the continuous curves $E(f)$ and $\eta(f)$, the full vibroacoustic model follows the measured on-axis SPL more closely than the constant-parameter model. The agreement is still not exact—consistent with the SPL-fitting limitations discussed above—but it is a clear improvement over the model with constant E and η.

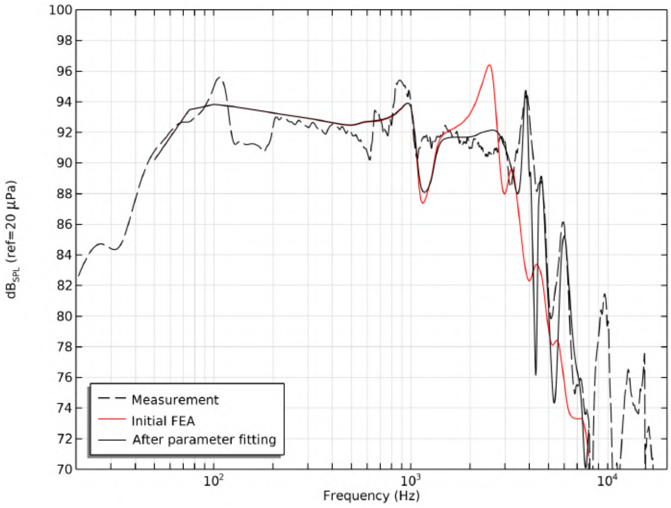

Figure 11: Validation (Study 12): on-axis SPL for the measurement, the constant-parameter model, and the model with the identified frequency-dependent $E(f)$ and $\eta(f)$.

V. Conclusions

This work identified the frequency-dependent Young's modulus $E(f)$ and isotropic loss factor $\eta(f)$ of the polypropylene cone of a 200 mm woofer by an inverse finite-element approach, using a 2D axisymmetric vibroacoustic model with a calibrated lumped-element drive and the measured on-axis SPL as the optimisation target. The suspension parameters were established first from electrical-impedance measurements, and a sensitivity analysis confirmed that the cone stiffness and damping dominate the response in the break-up region, justifying their identification from the radial break-up modes. Fitting the SPL band by band around each of the five break-up modes yielded effective E and η values which, interpolated into continuous curves, improved the agreement between simulation and measurement relative to a constant-parameter model.

The proposed model has, however, several limitations. The on-axis SPL is an accessible measurement, but its sensitivity to acoustic artefacts made the fit more difficult, particularly at higher frequencies; the identified cone parameters are effective rather than intrinsic, since they absorb the residual influence of the suspension and the simplifications of the model; and the impedance fit of the full suspension suggested that radiation damping of the air is missing from the structure-only studies.

Several lines of continuation follow naturally. The acoustic radiation loading could be included in the suspension identification to capture the missing damping. The SPL-based fit could be complemented, or cross-checked, with cone-acceleration data from a laser scanning vibrometer, combining the accuracy of the velocity measurement with the accessibility of the SPL. A larger number of modes, together with frequency-dependent suspension properties, would better constrain the identified curves. Finally, extending the model from a 2D axisymmetric to a full 3D geometry would allow the circumferential modes neglected here to be represented.

References

[1] J. D. Ferry, *Viscoelastic Properties of Polymers*, 3rd ed. New York: John Wiley & Sons, 1980.

[2] D. J. Ewins, *Modal Testing: Theory, Practice and Application*, 2nd ed. Research Studies Press, 2000.

[3] ASTM International, "ASTM E756-05(2023): Standard test method for measuring vibration-damping properties of materials," ASTM International, West Conshohocken, PA, Tech. Rep., 2023.

[4] W. Cardenas and W. Klippel, "Optimal material parameter estimation by fitting finite element simulations to loudspeaker measurements," in *Audio Engineering Society Convention 144*. Milan, Italy: Audio Engineering Society, May 2018, convention Paper 9928.

[5] W. Cardenas, "Modelling and measurement of nonlinear intermodal coupling in loudspeaker diaphragm vibrations," in *Audio Engineering Society Convention 147*. New York, NY, USA: Audio Engineering Society, Oct. 2019, convention Paper 10244.

[6] W. Klippel and J. Schlechter, "Distributed mechanical parameters of loudspeakers, part 1: Measurements," *Journal of the Audio Engineering Society*, vol. 57, no. 7/8, pp. 500–511, Aug. 2009.

[7] ——, "Distributed mechanical parameters of loudspeakers, part 2: Diagnostics," *Journal of the Audio Engineering Society*, vol. 57, no. 9, pp. 696–708, Sep. 2009.

[8] A. Replogle, "Advanced FEM simulation of loudspeaker performance: The impact of cone and surround materials," Master's thesis, Politecnico di Milano, Music and Acoustic Engineering, 2024, advisor: F. Antonacci; in collaboration with Faital S.p.A.

[9] G. Spatafora, E. Capucci, C. Corsini, and R. Toppi, "FEM simulations in loudspeakers design: Focus on mechanical and acoustical–structural analysis," in *Proceedings of the COMSOL Conference 2019*. Faital S.p.A., San Donato Milanese, Italy, 2019.

[10] M. Kim, J. Kook, P. R. Andersen, and I. Lee, "An automated framework for material property calibration in loudspeaker simulation models," 2024, preprint, SSRN 4841891.

[11] D. G. Nielsen, "Optimization of loudspeakers using material and shape optimization," Ph.D. thesis, Technical University of Denmark (DTU), 2021.

[12] A. W. Leissa, *Vibration of Plates*, ser. NASA SP-160. U.S. Government Printing Office, 1969.

[13] F. J. M. Frankort, "Vibration and sound radiation of loudspeaker cones," Ph.D. dissertation, Delft University of Technology, 1975, published in Philips Research Reports.

[14] M. I. Friswell and J. E. Mottershead, *Finite Element Model Updating in Structural Mechanics*. Kluwer Academic Publishers, 1995.

[15] J. B. Fahnline, R. L. Campbell, and S. A. Hambric, "Modal analysis using the singular value decomposition," Applied Research Laboratory, The Pennsylvania State University, Tech. Rep. Technical Report 04-008, 2004.

[16] M. Lee and M. Richardson, "Determining the accuracy of modal parameter estimation methods," in *Proceedings of the 10th International Modal Analysis Conference (IMAC X)*. Structural Measurement Systems, 1992.

[17] S. Mowry, "An engineering materials update, part 1," *Voice Coil*, 2008.

[18] A. Ricarte, J. Meireles, and O. Inácio, "Characterizing the frequency response of compliant materials by laser doppler vibrometry coupled acoustic excitation," *Vibration*, vol. 4, no. 1, pp. 64–74, 2021.

[19] *Structural Mechanics Module User's Guide*, COMSOL, 2024, version 6.4.